Analysis of the Impact of the Monitoring Equipment on the Common-Mode to Differential-Mode Conversion in Bulk Current Injection Tests

Pablo J. Gardella
Allegro Microsystems Argentina S.A.
Instituto Tecnológico de Buenos Aires (ITBA)
CABA, Argentina
pgardella@allegromicro.com
pgardell@itba.edu.ar

Eduardo Mariani
Allegro Microsystems Argentina S.A.
EM Ingeniería
CABA, Argentina
emariani.cw@allegromicro.com

***Abstract*—In this paper, the common-mode to differential-mode conversion in a Bulk Current Injection (BCI) test setup is analyzed in the presence of an optical fiber transmitter. A modular-basis analysis based on S-parameters measurements and Electromagnetic simulations has been performed. It is shown that the loading effects can change the insertion losses from the RF amplifier to the Devices Under Test, even at frequencies as low as 10MHz by 2dB and up to 23dB at worst cases. The study has been undertaken with the substitution and closed-loop methods. Quantification of this problem as well as mitigation strategies are proposed, analyzed and evaluated with the aim of improving the accuracy of BCI simulations at early-design stages. Considering the significant cost of redesigning at an advanced point in the product development cycle, the presented work expects to raise awareness about how even small changes in the BCI setup can remarkably compromise the outcome.**

***Index Terms*—Automotive EMC, Bulk Current Injection (BCI), common to differential mode conversion, ISO 11452, RF Immunity**

I. Introduction

In recent years, ElectroMagnetic Compatibility (EMC) has become increasingly important in the semiconductor industry, especially in the automotive market. Ongoing developments such as Internal Combustion Engines (ICE) with reduced CO_2 emissions, the Electric Vehicle (EV) and the Advanced Driver-Assistance Systems (ADAS), are demanding improvements not only in terms of EMC but also in regard to functional safety.

Among the many standards available concerning EMC, Bulk Current Injection (BCI) is one of the most common tests for characterizing the electromagnetic immunity of an automotive or an aerospace module/system to radiated interference [1]. The test setup is showed in Fig 1 and consists on the lumped-element model of a field-to-wire coupling by using a ferrite-based transformer as an injection probe [2]. A secondary probe can be used for measuring the effectively injected current in the wire harness that resembles the so-called closed-loop setup. During a BCI test, the injection probe delivers some amount of Common-Mode (CM) disturbance to the wiring harness, which leaks into a Differential-Mode (DM) due to the unbalances of the test setup, and can eventually be delivered to the Device Under Test (DUT). This CM-to-DM conversion is one of the most critical parameters in BCI, since DUTs are susceptible to the DM rather than to the CM [3]–[6].

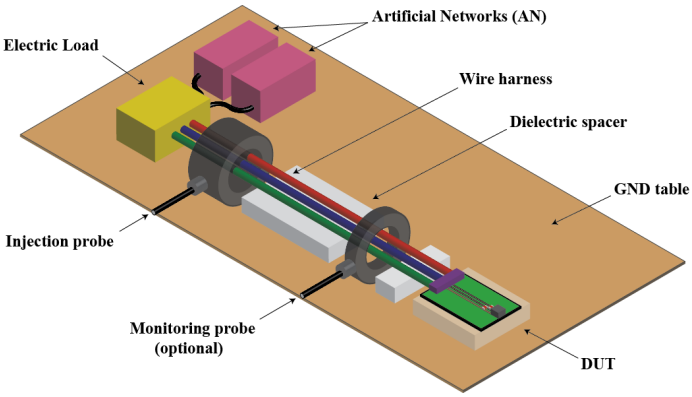

Fig. 1: Schematic representation of a typical BCI test setup. The figure is not to scale.

System-level tests like BCI are meant to mimic real-life scenarios by providing, for example, harness resonances and load circuits similar to the ones that will be employed by the Engine Control Unit (ECU) to communicate with the ICs in the actual environment. On the other hand, IC-level tests have proven to be of great importance in providing fair metrics for quantifying immunity and emissions of a bare IC to either conducted or radiated Electromagnetic Interference (EMI) [7]. As showed in [8] it is possible to translate from one to another by using S-parameters models. This real-world correlation of the system-level tests instead of the "laboratory conditions" of IC-levels, makes the modeling of the former much more challenging than the latter. Moreover, having accurate models of these test setups is of paramount importance in the industry, since it allows IC designers to simulate these tests at early stages, which minimizes the risks associated with expensive

and belatedly redesigns that may prevent to accomplish the expected times-to-market.

During EMC tests performed inside a Faraday cage, like BCI, the monitoring of the DUTs is typically carried out by optical means. A transmitter is placed inside the chamber to convey the output signal while minimizing cross-talk between inner and outer sides. On this subject, the International Organization for Standardization (ISO) standard 11452-4 [1] recommends that for BCI the DUT monitoring *"may be accomplished by using fiber-optics, or high-resistance leads. Other type of leads may be used but require extreme care to minimize interactions. The orientation, length and location of such leads shall be carefully documented to ensure repeatability of test results. Any electrical connection of monitoring equipment to the DUT may cause malfunctions of the DUT. Extreme care shall be taken to avoid such an effect"*. On the other hand, technology trends have been pushing the developments of Systems-on-Chip (SoC) structures, in which two dice may be placed inside a single package for redundancy purposes, usually driven by functional safety requirements. These situations, where two devices may be active during a test, are not being taken into account by the ISO standard, which leaves undefined, for example, whether the devices must be simultaneously monitored or not.

EMC tests in general, and BCI in particular, are typically modeled by a divide-and-conquer strategy [4]. Considering a single-ended Quasi-Transverse ElectroMagnetic (QTEM) propagation mode on each of the cables, the test setups can be splitted in common elementary blocks which not only reduces the computational time and memory requirements for ElectroMagnetic (EM) simulations, but also maximizes reusability for different DUTs and test setups. Even though the modeling of these fundamental blocks have been extensively studied by many groups [4]–[6], [9], [10], the authors of this work have not been able to find in the state-of-the-art any quantitative nor qualitative study of the effects that the monitoring equipment can impair into the CM-to-DM conversion in a real BCI test setup. If this is not taken into account, the correlation between BCI simulations and measurements may get compromised, consequently degrading the accuracy of these highly-appreciated early predictions even at frequencies as low as 10MHz. For that reason, this work analyzes the impact of the widely established optical-fiber transmitters into the CM-to-DM conversion of some typical BCI test setups with special emphasis in real-life situations.

In the first section, the different test setups and their building blocks will be described. Secondly, the impedance model for a generic monitoring equipment will be developed. And finally, measurements of a commercially available transmitter and the simulated CM-to-DM conversions will be showed.

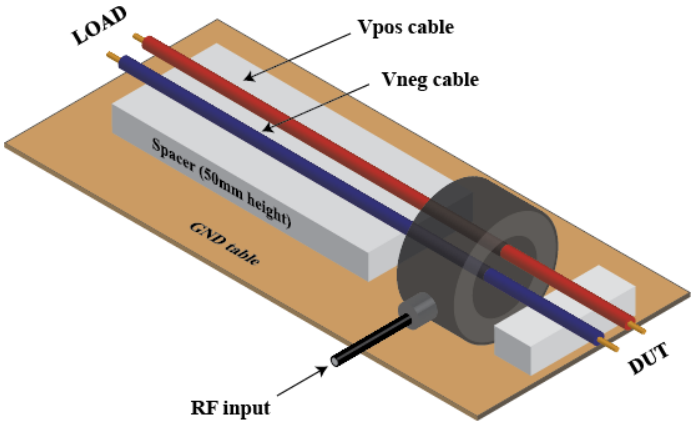

Fig. 2: Schematic representation of a 2-wire BCI harness under the substitution method. The figure is not to scale.

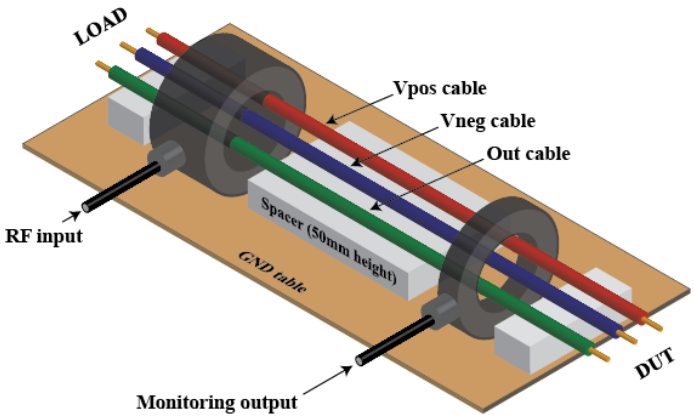

Fig. 3: Schematic representation of a 3-wire BCI harness under the closed-loop method. The figure is not to scale.

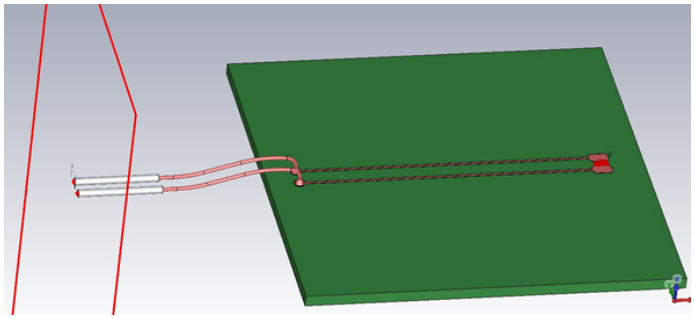

Fig. 4: EM model of the PCB for the 2-wire case. The perpendicular plane on the left indicates where the two QTEM ports are, while the two pads on the right constitute the floating lumped port for the 2-pins IC.

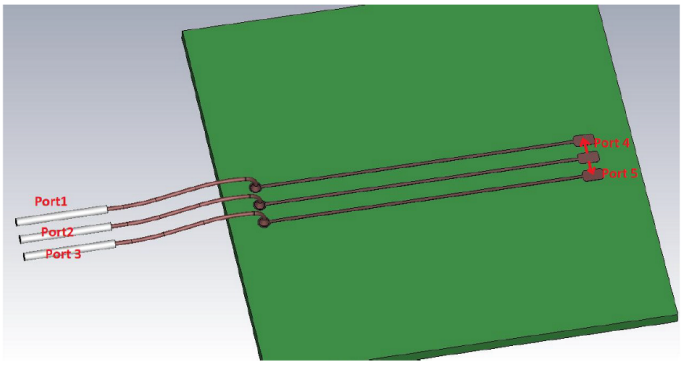

Fig. 5: EM model of the 3-wire PCB. The connectors on the left are three QTEM ports while the three pads on the right constitute the two floating lumped ports for the 3-pins IC.

II. BCI TEST SETUPS

The analysis has been performed using a modular approach where the reference of each block is the system GND. The following subsections describe how each of the modules has been modeled and studied.

A. Harnesses

Two different scenarios have been analyzed: an open-loop (or substitution) 2000mm-length untwisted 2-wire harness with the injection probe FCC F-140 placed at 450mm from the DUT and a closed-loop 1000mm-length untwisted 3-wire harness with the injection probe at 900mm and the monitoring probe FCC F-65 placed at 50mm from the DUT.

The first setup is showed in Fig 2. Given that the output magnitude is the IC's current, the sensing element is typically a 50Ω or 100Ω resistor with a nF capacitor. Secondly, the 3-wire harness presented in Fig 3 has an output driver that operates in the voltage domain. Examples of these situations are open-drain or push-pull stages where the load element is typically a pull-up/down resistor in the units of $k\Omega$ with a capacitor in the same range as in the 2-wire case.

B. DUT

The DUTs are 50mm x 50mm PCBs (FR4, 1.6mm) with the layouts showed in Fig. 4 for the 2-wire case and in Fig. 5 for the 3-wire. The EM simulations have been performed using CST Studio as the frequency domain solver with an input QTEM port for each wire [4]. The bottom layer is a GND plane connected to the GND pin at the input pads and the IC is connected to lumped floating ports on the opposite side of the boards.

For the subsequent circuit simulations, the IC is replaced by a lumped 100nF SMD by-pass capacitor (ESL=1nH, ESR=0.1Ω) in parallel with a 50Ω resistor acting as the receiving load. The 3-wire case has the same RC load for both Vpos-Vneg and Out-Vneg ports.

C. Loads and Artificial Network

The Artificial Network (AN) is a Schwarzbeck NNBM 8124-200N in agreement with [1], whose 1-port S-parameter matrix has been measured with a Vector Network Analyzer (VNA) PicoVNA2 between 1MHz and 400MHz.

The electric load in the case of the 2-wire harness is a lumped 100Ω resistor in parallel with a $1nF$ capacitor (ESL=1nH, ESR=0.1Ω), connected between one AN and the Vneg cable coming from the DUT. On the other hand, the load for the 3-wire case is a lumped $1k\Omega$ resistor connected between the Out and Vpos cables and $1nF$ capacitor connected between the Out and Vneg cables.

III. MONITORING EQUIPMENT MODELING

The optical fiber transmitter studied in this work is a Messtechnik U1/12 and is showed in Fig. 6a. It has a BNC input connector with positive (inner) and negative (outer) conductors. There is also an external Anti-Alias Filter (AAF) with $-3dB@1MHz$ and some non-RF cables to connect to the load circuit. It is important to highlight the inherent asymmetry due to the non-balanced input terminals.

The input DM impedance of the transmitter is specified as $8pF//1M\Omega$ while the CM impedance is usually not detailed due to its setup-dependence. In this work, the following situations have been analyzed to determine the different contributions of the capacitive effects to the GND plane:

1) Transmitter standing on the GND plane.
2) Metallic support (h=25mm, galvanized steel).
3) Polystyrene support (h=25mm, $\epsilon_r \approx 1.1$).

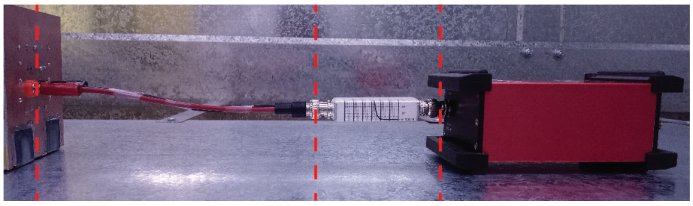

(a) Situation 1. Optical-Fiber module with the transmitter on the right, the AAF in the middle and the non-RF cables with the measurement fixture on the left. The red lines indicate the calibration planes.

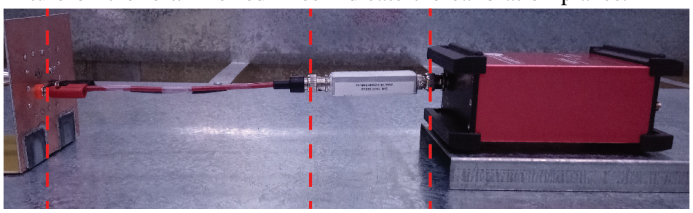

(b) Situation 2. The support is 25mm-height to keep the cables at 50mm from the GND table. Compared to situation 1, only the cables and the AAF have changed their interaction with the plane.

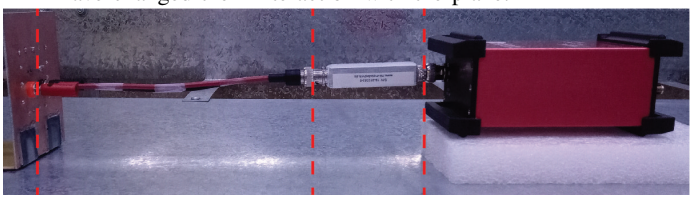

(c) Situation 3. Compared to situation 2, only the transmitter has changed its interaction with the plane.

Fig. 6: Setups for characterizing the monitoring equipment.

The responses have been characterized with a 2-port VNA, each one of those connected to the input lines (the positive and the negative terminals) by means of a vertical fixture as the one showed in Fig. 6a. The 2-port S-parameters matrices have been converted to their impedance equivalence with the well-known relationships, leading to the following system. The port 1 has been arbitrarily assigned to the internal conductor and port 2 to the external.

$$\vec{V} = Z \cdot \vec{I} \quad \rightarrow \quad \begin{bmatrix} V_1 \\ V_2 \end{bmatrix} = \begin{bmatrix} Z_{11} & Z_{12} \\ Z_{21} & Z_{22} \end{bmatrix} \cdot \begin{bmatrix} I_1 \\ I_2 \end{bmatrix} \tag{1}$$

The modal voltages ($\vec{V}_m$) can be related to the pin voltages by the matrix M_V and the modal currents ($\vec{I}_m$) to the pin currents by the matrix M_I.

$$\vec{V}_m = M_V \cdot \vec{V} \quad \rightarrow \quad \begin{bmatrix} V_{DM} \\ V_{CM} \end{bmatrix} = \begin{bmatrix} 1 & -1 \\ \frac{1}{2} & \frac{1}{2} \end{bmatrix} \cdot \begin{bmatrix} V_1 \\ V_2 \end{bmatrix} \tag{2}$$

$$\vec{I}_m = M_I \cdot \vec{I} \quad \rightarrow \quad \begin{bmatrix} I_{DM} \\ I_{CM} \end{bmatrix} = \begin{bmatrix} \frac{1}{2} & -\frac{1}{2} \\ 1 & 1 \end{bmatrix} \cdot \begin{bmatrix} I_1 \\ I_2 \end{bmatrix} \tag{3}$$

Then, as shown by [11], the modal Z-parameters matrix (Z_m) can be expressed in terms of the single-ended Z-parameters matrix and the modal-conversion matrices.

$$Z_m = M_V \cdot Z \cdot M_I^{-1} \tag{4}$$

$$\vec{V}_m = Z_m \cdot \vec{I}_m \rightarrow \begin{bmatrix} V_{DM} \\ V_{CM} \end{bmatrix} = \begin{bmatrix} Z_{DM} & Z_{DC} \\ Z_{CD} & Z_{CM} \end{bmatrix} \cdot \begin{bmatrix} I_{DM} \\ I_{CM} \end{bmatrix} \tag{5}$$

$$Z_m = \begin{bmatrix} Z_{11} - Z_{21} - Z_{12} + Z_{22} & \frac{Z_{11} - Z_{21} + Z_{12} - Z_{22}}{2} \\ \frac{Z_{11} + Z_{21} - Z_{12} - Z_{22}}{2} & \frac{Z_{11} + Z_{21} + Z_{12} + Z_{22}}{4} \end{bmatrix} \tag{6}$$

Since the network is reciprocal ($Z_{12} = Z_{21}$), the CM-to-DM conversion is equal to the DM-to-CM conversion, but this quantity is not zero due to the asymmetric structure of the module, where the negative terminal is much more exposed to the GND plane than the inner conductor ($Z_{11} \neq Z_{22}$).

Therefore, the modal Z-parameters for a reciprocal and asymmetric 2-port network are:

$$\begin{cases} Z_{DM} = Z_{11} - 2 \cdot Z_{21} + Z_{22} \\ Z_{CM} = \frac{Z_{11} + 2 \cdot Z_{21} + Z_{22}}{4} \\ Z_{CD} = Z_{DC} = \frac{Z_{11} - Z_{22}}{2} \end{cases} \tag{7}$$

The equivalent circuit to the modal parameters proposed in [11] is showed in Fig. 7, where the mode-conversion is being captured by the impedance Z_{DC}.

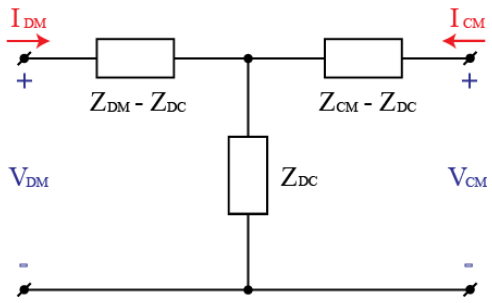

Fig. 7: Representation of a passive 2-port network in terms of modal Z-parameters.

IV. Results

A. Impedance measurements

The module response has been measured in the situations presented in Fig. 6a, 6b and 6c. Their S-parameters have been converted into modal Z-parameters following Section III steps. The transmitter's DM impedance is showed in Fig. 8 where the effects of the AAF and the non-RF cables have been isolated. The impedances are showed in Figs. 9, 10 and 11. It can be noticed that the benefit of the polystyrene support is twofold: on the one hand, it is the only situation in which the CM impedance increases (capacitive effects of the transmitter are dominating the CM impedance of the entire module), and on the other hand, it also reduces the mode conversion while keeping the DM impedance unaffected.

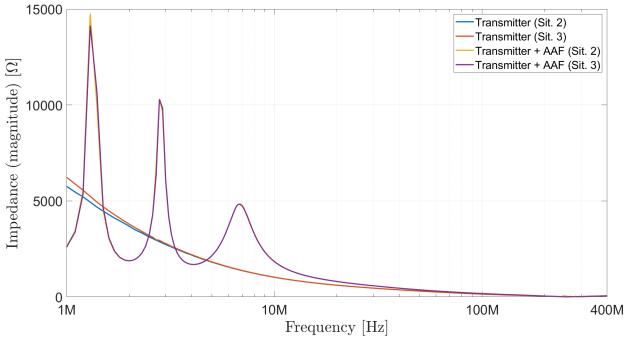

Fig. 8: Z_{DM} of transmitter and AAF at the calibration planes. The peaks are given by the AAF's zeros on the rejection band.

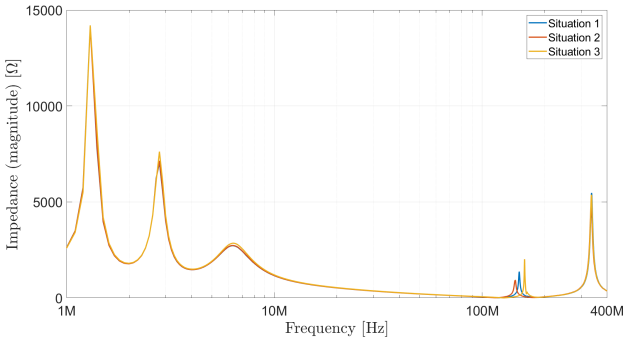

Fig. 9: Z_{DM} in the different situations.

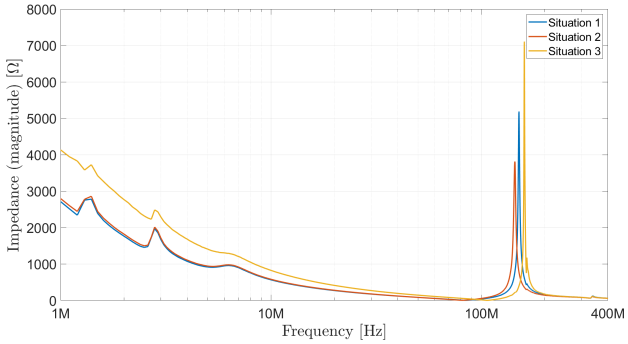

Fig. 10: Z_{CM} in the different situations.

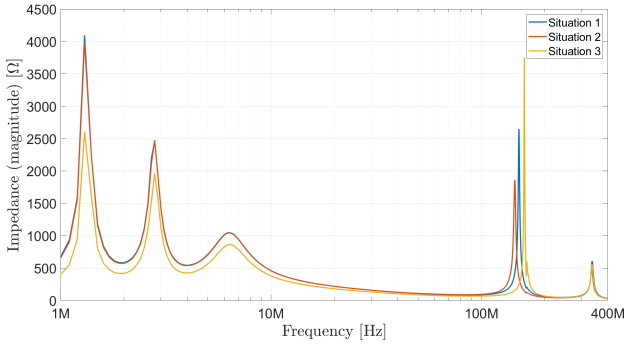

Fig. 11: Z_{DC} in the different situations.

B. System-level BCI simulation

To quantify the CM-to-DM conversion, the 50Ω resistor at the Vpos-Vneg port has been taken as the output and insertion losses simulations have been carried out with the test-benches showed in Fig. 12 and Fig. 13. All S-parameters, either simulated or characterized, have been incorporated as Touchstone files into the Cadence simulator.

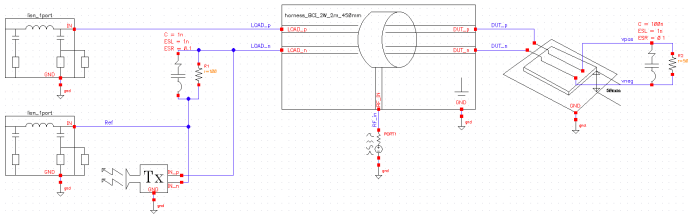

Fig. 12: Virtual environment for the 2-wire BCI simulation.

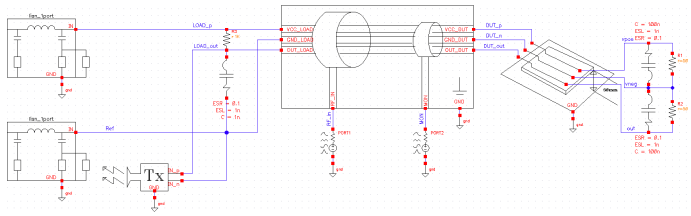

Fig. 13: Virtual environment for the 3-wire BCI simulation.

Figs. 14 - 16 prove the addition of the monitoring equipment can change the CM-to-DM conversion. In sit. 1, the differences with the ideal case for the 2-wire setup are 8dB@10MHz and 19dB@50MHz as the Worst Cases (WC). Changing to sit. 3 reduces them to 5dB and 11dB respectively. On the other hand, for the 3-wire harness the discrepancies on the Vpos-Vneg port are 1.7dB@40MHz and 15dB@80MHz as WC, while in sit. 3 they become 0.7dB and 23dB respectively. For the Out-Vneg port they are 2.6dB@20MHz and 5dB@80MHz as WC, while for sit. 3 they change to 1.2dB and 10dB respectively. It is worth noting that a larger CM impedance is no guarantee of lower variations. Even though there are more impedance discrepancies below 10MHz, the CM-to-DM conversion remains the same below such frequency due to the effectiveness of the capacitors below their self-resonance.

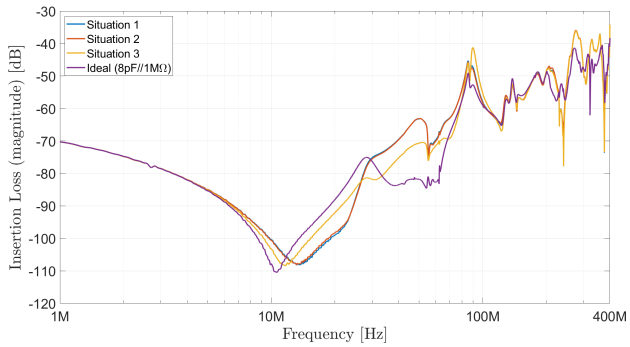

Fig. 14: CM-to-DM conversion in the 2-wire case.

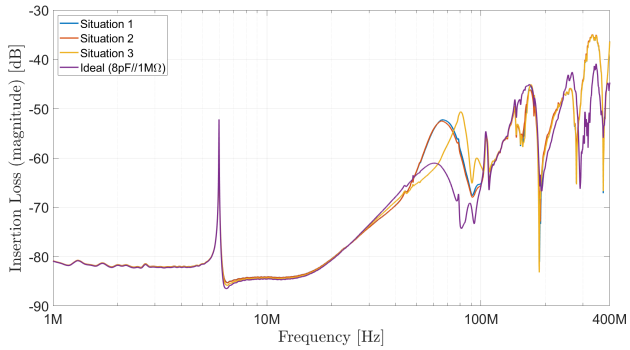

Fig. 15: CM-to-DM conversion in the 3-wire case (Vpos-Vneg). The low-frequency peak is the load capacitor resonating with the harness inductance.

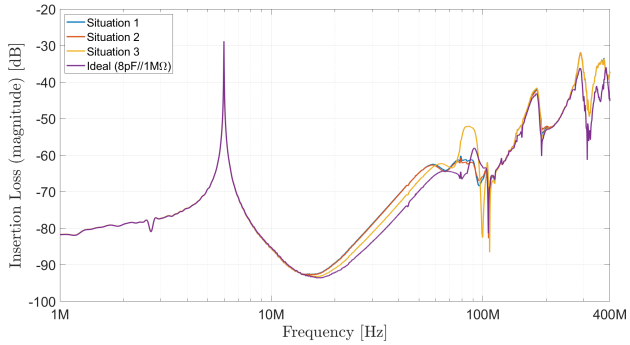

Fig. 16: CM-to-DM conversion in the 3-wire case (Out-Vneg).

V. Discussion

Similarly to the uncertainty principle, when loading a BCI test setup with a monitoring equipment, the behavior of the observed object will change. Therefore, disregarding this loading may attempt to compromise not only reproducibility (if test conditions are not properly documented), but also the accuracy of the early-design stage simulations in predicting the power delivered to a certain load.

In the present paper, certain scenarios have been proposed and studied to determine the modal impedances of an optical fiber transmitter. Differences on the CM-to-DM conversion of BCI test setups have been quantified between 2dB and 23dB. Although adequate filtering can mitigate these effects, since their bandwidth is limited, BCI simulations shall take them into account for better accuracy throughout the entire spectrum.

Even though the quantitative analysis presented in Section IV is highly-dependent on these particular case-studies, this proof of concept is completely applicable to any situation, and the authors insist on the importance of considering such effects for accurate simulations. Moreover, since this loading will happen regardless of the harness length, the probes positions and the monitoring probe presence, similar behaviors are expected in other cases. Therefore these results can be qualitatively extrapolated to other situations.

Besides that, it is important to highlight that the ISO 11452-4 standard [1] defines the "testbench transfer impedance" as the CM voltage in the injector probe position, divided by the CM current at the measuring probe position. On top of being a fingerprint of the actual testbench, which is significantly useful for comparison among test setups (and facilities), it inherently incorporates the effects of the monitoring equipment. However, as showed by [12] many concerns can be raised regarding the use of it due to the several approximations and high-frequency limitations. Nevertheless, it is indeed a useful metric for test setups comparisons (given a same set of DUT and load circuit) and the authors encourage the use of it for guaranteeing a better control of the actual test setup conditions.

As a corollary of these outcomes, and in regard to the SoC case-study, it is worth mentioning that the ISO 11452-4 standard [1] does not outline situations where two or more devices may be active during a test, leaving that up to the test plan agreed between suppliers and customers. Owing to the reasons explained in this paper, it is of utmost importance that the monitoring equipment does not degrade the BCI signature by loading one output at a time. Otherwise, inaccurate simulations and testing may occur. Thus, the authors encourage the simultaneous monitoring of all the outputs meant to be used by the ECU during a real-life situation.

VI. Conclusions

In the present work, the impact of the monitoring equipment into the CM-to-DM conversion in BCI test setups has been analyzed and evaluated. It has been shown that even commercially available equipment, specifically designed for EMC tests, can load and change results, in particular when they have non-RF and unbalanced interfaces.

In order to consider these effects and mitigate correlation discrepancies, the authors recommend the use of the testbench transfer impedance as a fingerprint of the BCI test setup. Otherwise, such effects can be directly translated into a lack of accuracy during the early-design stage simulations.

Last but not least, addition of guidelines regarding the correct use of the monitoring equipment and SoC structures is encouraged for future revisions of [1].

Acknowledgments

Eduardo Mariani is an exclusive consultant of Allegro Microsystems Argentina S.A. The authors would like to thank Andrés Altieri for his support with the EM simulations.

References

[1] ISO 11452-4 (2020): Road Vehicles-Component Test Methods for Electrical Disturbances by Narrowband Radiated Electromagnetic Energy Part 4: Bulk Current Injection (BCI)

[2] S. Pignari and F. G. Canavero, "Theoretical assessment of bulk current injection versus radiation," in IEEE Transactions on Electromagnetic Compatibility, vol. 38, no. 3, pp. 469-477, Aug. 1996, doi: 10.1109/15.536077.

[3] P. S. Crovetti and F. Fiori, "Distributed Conversion of Common-Mode Into Differential-Mode Interference," in IEEE Transactions on Microwave Theory and Techniques, vol. 59, no. 8, pp. 2140-2150, Aug. 2011, doi: 10.1109/TMTT.2011.2144994.

[4] Y. Kondo, M. Izumichi and O. Wada, "Simulation of Bulk Current Injection Test for Automotive Components Using Electromagnetic Analysis," in IEEE Transactions on Electromagnetic Compatibility, vol. 60, no. 4, pp. 866-874, Aug. 2018, doi: 10.1109/TEMC.2017.2751580.

[5] S. Miropolsky, A. Sapadinsky and S. Frei, "A generalized accurate modelling method for automotive bulk current injection (BCI) test setups up to 1 GHz," 2013 9th International Workshop on Electromagnetic Compatibility of Integrated Circuits (EMC Compo), Nara, 2013, pp. 63-68, doi: 10.1109/EMCCompo.2013.6735174.

[6] S. Miropolsky, S. Jahn, F. Klotz and S. Frei, "Experimental validation of the generalized accurate modelling method for system-level bulk current injection setups up to 1 GHz," 2015 10th International Workshop on the Electromagnetic Compatibility of Integrated Circuits (EMC Compo), Edinburgh, 2015, pp. 137-142, doi: 10.1109/EMCCompo.2015.7358345.

[7] T. Steinecke et al., "Generic IC EMC Test Specification," 2012 Asia-Pacific Symposium on Electromagnetic Compatibility, Singapore, 2012, pp. 5-8, doi: 10.1109/APEMC.2012.6237982.

[8] H. Pues et al., "Translation of automotive module RF immunity test limits into equivalent IC test limits using S-parameter IC models," 2013 9th International Workshop on Electromagnetic Compatibility of Integrated Circuits (EMC Compo), Nara, 2013, pp. 249-253, doi: 10.1109/EMCCompo.2013.6735209.

[9] F. Grassi, F. Marliani and S. A. Pignari, "Circuit Modeling of Injection Probes for Bulk Current Injection," in IEEE Transactions on Electromagnetic Compatibility, vol. 49, no. 3, pp. 563-576, Aug. 2007, doi: 10.1109/TEMC.2007.902385.

[10] A. Durier, H. Pues, D. Vande Ginste, M. Chernobryvko, C. Gazda and H. Rogier, "Novel modeling strategy for a BCI set-up applied in an automotive application: An industrial way to use EM simulation tools to help hardware and ASIC designers to improve their designs for immunity tests," 2011 8th Workshop on Electromagnetic Compatibility of Integrated Circuits, Dubrovnik, 2011, pp. 41-46.

[11] H. Cheaito, M. Diop, M. Ali, E. Clavel, C. Vollaire and L. Mutel, "Virtual Bulk Current Injection: Modeling EUT for Several Setups and Quantification of CM-to-DM Conversion," in IEEE Transactions on Electromagnetic Compatibility, vol. 59, no. 3, pp. 835-844, June 2017, doi: 10.1109/TEMC.2016.2631721.

[12] P. S. Crovetti and F. Fiori, "A Critical Assessment of the Closed-Loop Bulk Current Injection Immunity Test Performed in Compliance With ISO 11452-4," in IEEE Transactions on Instrumentation and Measurement, vol. 60, no. 4, pp. 1291-1297, April 2011, doi: 10.1109/TIM.2010.2084870.